Cross Sections for X-Ray Photoelectron-Induced Desorption of Hydrogen Ions from Metal Surfaces

J. H. Kinney

W. J. Siekhaus

R. A. Anderson

September 20, 1985

Lawrence Livermore National Laboratory

CROSS SECTIONS FOR X-RAY PHOTOELECTRON-INDUCED
DESORPTION OF HYDROGEN IONS FROM METAL SURFACES

ABSTRACT

We have measured the cross sections for x-ray photoelectron-induced desorption of hydrogen ions from beryllium, carbon, aluminum, tantalum, and gold surfaces. This report describes the results of the cross-section measurements, and discusses a time-of-flight technique that allows the determination of ionic-desorption cross sections as small as 10^{-25} cm^2 per photoelectron.

1. INTRODUCTION

The measurement of the photoelectron-induced desorption cross sections for both ions and neutrals is of practical importance in a large number of emerging technologies. For example, the vacuum designs for synchrotrons and for fusion energy machines depend critically on the gas loads produced from photoelectron desorption. Also, the interpretation of many weapon experiments requires at least a rough estimate of x-ray-induced particle emission.

With the exception of an earlier study by Brumbach and Kaminsky,[1] few measurements of x-ray photoelectron desorption have been made. In Brumbach's work, only the desorption of CO molecules was considered. We have chosen to measure the x-ray photoelectron desorption cross sections of H^+ off of metal surfaces because (1) few accurate measurements have been reported, (2) H^+ is one of the larger single species of desorbed ion, and (3) H^+ is one of the more difficult ions to detect using standard mass spectroscopic techniques.

This report is divided into four sections. In Section 2 we describe the x-ray source used, and also give details of the time-of-flight detector. In Section 3 the measured desorption cross sections from beryllium, carbon, aluminum, tantalum, and gold surfaces are given. In Section 4 we discuss the measured cross sections in terms of current models of electron-impact desorption and compare the results with cross sections obtained by other workers using energy electrons.

2. EXPERIMENTAL APPARATUS

THE X-RAY SOURCE

Time-of-flight spectroscopy requires that the production of ions occurs over a time that is short with respect to the separation in time of the ion masses that are to be identified. Furthermore, since ion desorption cross sections are very small, it is desirable that the current that produces the ions be large in order to obtain detectable signals.

A Field Emission Corporation Febetron, which meets both of these requirements, was a natural choice as an x-ray source for these experiments. The Febetron emits a high-current (4000 A) narrow-pulse (5 ns) burst of electrons with energies spread between 100 and 600 keV. Figure 1 shows the measured electron energy spectrum produced by the Febetron used in this study.[2]
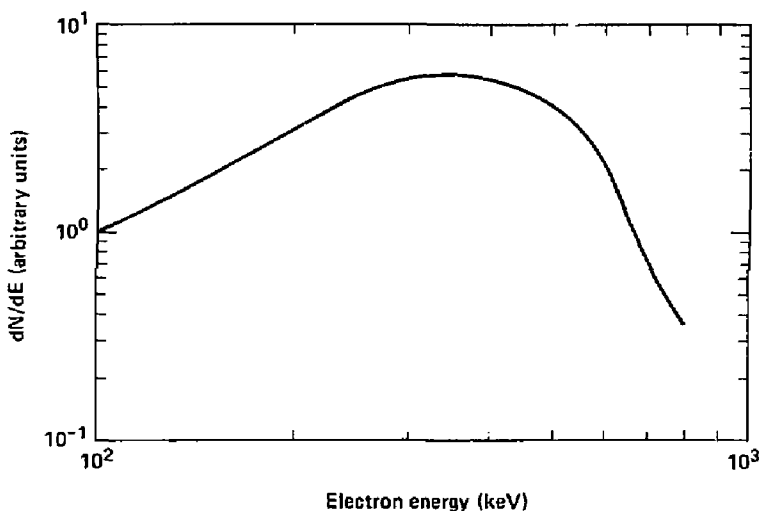

Fig. 1. The distribution in energy of electrons emitted from the Febetron. The appearance of electrons with energies greater than 600 keV may not be real; rather, the signal may be due to inadequate shielding of the pin diode detectors.
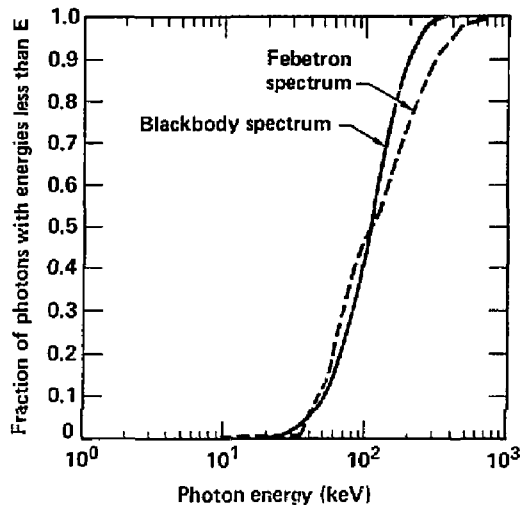
Fig. 2. The calculated integral of the x-ray spectrum generated by the Febetron. For comparison, a calculated integral 30-keV blackbody x-ray spectrum is shown. The blackbody spectrum has passed through a 0.005-in. tantalum target.

In this experiment, the field-emitted electrons from the Febetron are focussed onto a 0.005-in.-thick tantalum disk. This produces an intense, thick-target bremsstrahlung spectrum, which has been calculated using Monte Carlo techniques.[3] The result of the calculation of the x-ray spectrum is shown in Fig. 2. For comparison, we have also calculated the x-ray spectrum produced by a 30-keV blackbody radiator.[4] The spectra in Fig. 2 are integral spectra that have been normalized to 1.

THE TIME-OF-FLIGHT ASSEMBLY

The time-of-flight assembly is shown in Fig. 3. This assembly consists of three components: an extraction grid, a focussing cylinder lens, and a saddle field lens. Also shown in this figure are the electron drift tube emerging from the Febetron, the hard tantalum aperture used for collimation of the incident electron beam, the tantalum x-ray production plate, and the microchannel plate detector.
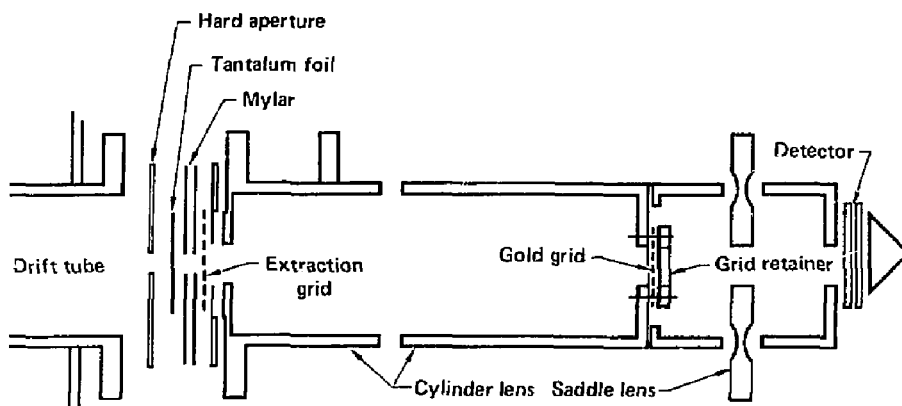
3

Fig. 3. The time-of-flight assembly used in this experiment.

The extraction grid is biased at -400 V during operation. Its purpose is to extract and accelerate positive ions from the target surface. It also reduces the angular divergence of the desorbed ions. The cylindrical lens is used to focus the ions toward the detector. The front end of the lens is biased the same as the extraction grid (-400 V). The second stage is biased at -2000 V. The saddle lens is at ground potential. Its purpose is to remove all ions that are not desorbed from the surface.

A simple calculation shows why the removal of all ions not originating at the surface was necessary for this study. First, the concentration of gas molecules per cubic centimeter at pressure P is approximately

$$C = 3.6 \times 10^{16} \, P \quad , \tag{1}$$

where P is in torr. The operating pressure during this series of experiments was 3×10^{-6} torr, indicating a volume concentration of $\sim 10^{11}$ atoms/cm^3. The surface concentration of hydrogen atoms was of the order 10^{15}/cm^2. Since the ionization volume for the photoelectron beam produced by the configuration of this detector is of the order of 10 cm^3, the surface desorption cross sections cannot be less than 10^{-3} times the volume gas ionization cross sections in order to be uniquely resolved above background.

4

Because the volume ionization cross section is of the order of 10^{-19} cm^2, a time-of-flight detector that does not discriminate between volume and surface ions will not resolve desorption cross sections smaller than 10^{-22} cm^2 at the pressures realized in this experiment.

In order to measure cross sections smaller than 10^{-22} cm^2, steps had to be taken to reduce the ionization volume. This was the purpose of the extraction grid and saddle lens. Figure 4 shows the potential energy along the z-axis of the time-of-flight tube from the target to the detector. It is apparent from energy considerations that any particle that is not ionized between the target and the extraction grid cannot surmount the saddle point. This effectively reduces the ionization volume by three orders of magnitude, which gives a detectable cross-section limit of 10^{-24} cm^2. Furthermore, the volume background signal is easy to separate from the surface signal because the linear potential gradient between the extraction grid and the target spreads the volume background signal out in time. Under present
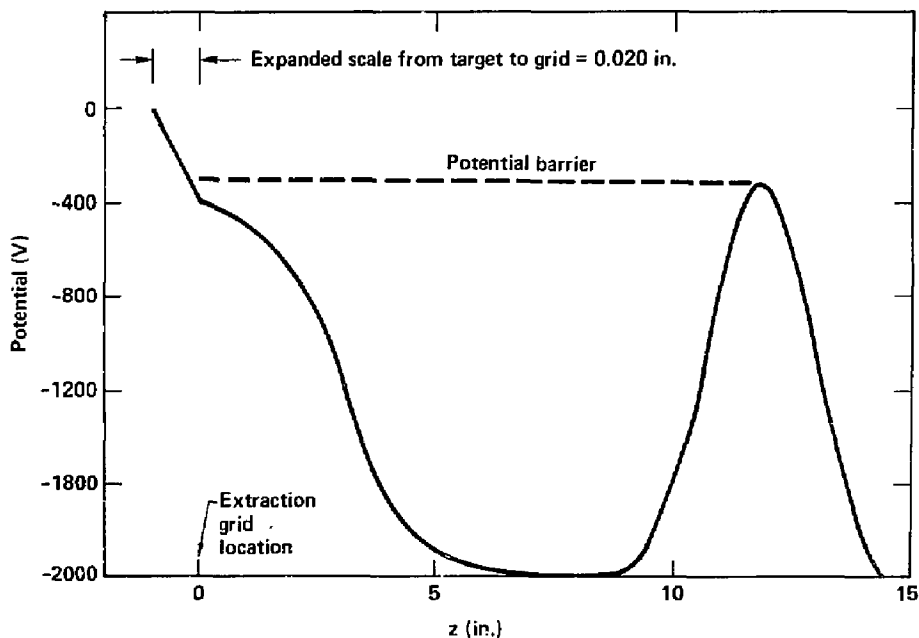

Fig. 4. Potential along the center axis (r = 0) of the time-of-flight tube.

operating conditions it is possible to measure cross sections as low as 10^{-25} cm^2. With an improved vacuum, we expect to be limited only by the gain of the detector ($<10^{-26}$ cm^2).

Figure 5 shows the calculated potential contours for this time-of-flight assembly. Some sample proton trajectories, shown in Fig. 5b, demonstrate that only ions generated in the vicinity of the surface can reach the detector and that all other ions are turned back at the saddle point.

THE DETECTOR

The detector consists of two microchannel plates mounted in a chevron-pair configuration[5] coupled to an impedance matched 50Ω metal anode. The gain of the detector, which was determined using a ^{22}Na source in a single-particle count mode, is 1.2 X 10^7 when a differential plate voltage of 1000 V per plate is applied.

Microchannel plate detectors have advantages over other types of detectors in this particular experimental configuration. Chief among these advantages is the ability to turn the plates on very rapidly. If the plates are left on during the initial x-ray pulse, the high flux of photoelectrons hitting the detector quickly saturates the plates and makes them inoperative. Therefore, the channel plates are left off for the first 400 ns after the Febetron discharges, giving the electrons a chance to disappear. The plates are turned on just prior to the proton arrival. Because of the two grids between the time-of-flight tube and the detector, the plates can be turned on without affecting the trajectories of the ions.

Approximately 10^3 protons arrive at the face of the first channel plate from a typical x-ray burst. The time spread is of the order of 10^{-8} s, corresponding to a count rate of 10^{11} counts/s. Since this count rate is much too fast to measure in a single-particle mode, the voltage spike at the anode is integrated to give the measured charge, Q_m:

$$Q_m = \frac{1}{50} \int_t V(t)\, dt \quad . \tag{2}$$

The number of protons desorbed from the surface, $Q*$, is

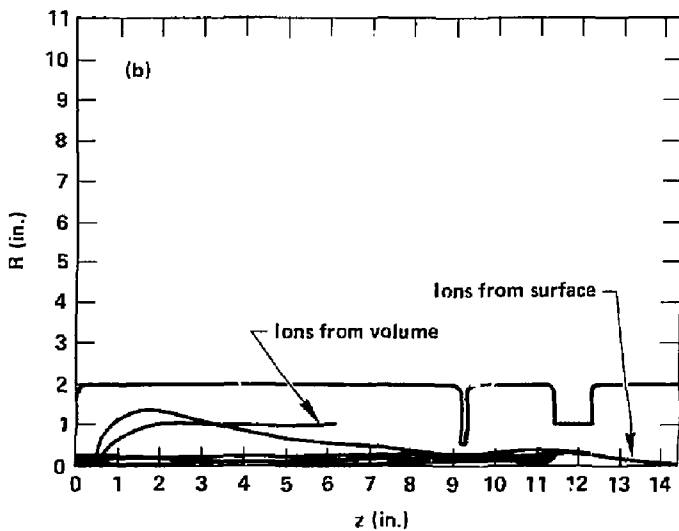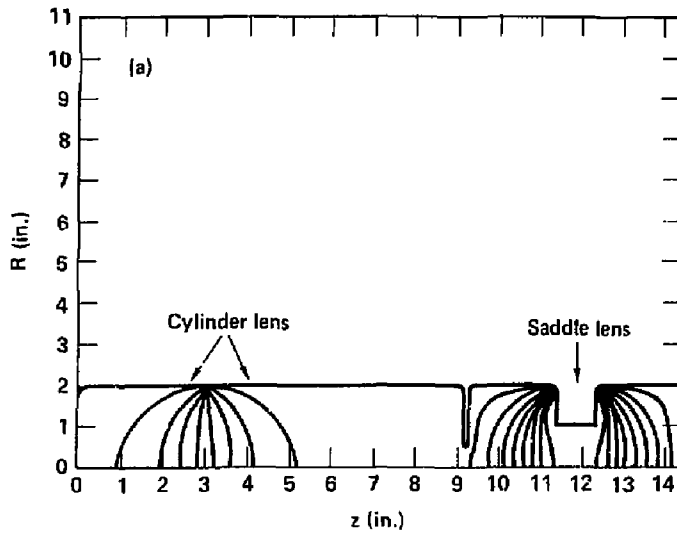$$Q* = \frac{Q_m}{Ge T_1 T_2} \quad , \tag{3}$$

6

Fig. 5. (a) Potential energy contours calculated for this lens.
(b) Trajectories are plotted for hydrogen atoms that have been ionized at the
surface and within the volume. Note that protons that have originated to the
right of the extraction grid are turned back at the saddle lens.

where G is the detector gain (1.2×10^7), ϵ is the detector efficiency (0.5), and T_1 and T_2 are the transmission factors of the first and second grids, respectfully.

The largest source of error in Eq. (3) lies in choosing the appropriate value for ϵ, the detector efficiency. This is because the efficiency is not measured directly during the gain measurements. Instead, the ratio of active channel area to total detector area is used for the efficiency factor. At the low proton energies in this experiment, this assumption is not unreasonable.[5] Another possible source of error lies in the assumption that no protons are lost by collisions with the detector walls. Trajectory calculations, however, indicate that this does not occur.

3. EXPERIMENTAL PROCEDURE AND RESULTS

Samples of beryllium, carbon, aluminum, tantalum, and gold in the form of high-purity 1-μm-thick coatings were sputter-deposited onto 5-mil tantalum foils. These deposited tantalum foils were sandwiched between the hard tantalum aperture and the extraction grid as shown in Fig. 3, and mounted together with the detector on the vacuum side of the Febetron drift tube. The assembly was then evacuated to a nominal pressure of 3×10^{-6} torr.

Time-of-flight mass spectra were recorded by firing the Febetron and using the electromagnetic pulse from the electrons to trigger both the turn-on of the channel plates and the oscilloscope sweeps. An array of 7912AD digitizing oscilloscopes recorded the sweeps. The anode voltage response (mass scans) and a corresponding x-ray diode signal were digitized and put on computer files for later analysis. The total number of protons released from the sample during a shot was determined using Eq. (3).

In order to obtain absolute photoelectron desorption cross sections, it is necessary to calibrate the x-ray diode response measured during mass scans to the total number of photoelectrons passing through the sample. This calibration is done by sealing off the time-of-flight tube so that no electrons can escape, and then measuring the voltage induced during several shots. The total photoelectron charge is determined using the relation

$$Q_{pe} = CV \quad , \tag{4}$$

where C is the measured capacitance of the assembly and V is the voltage difference between the grounded sample and the time-of-flight tube. A typical
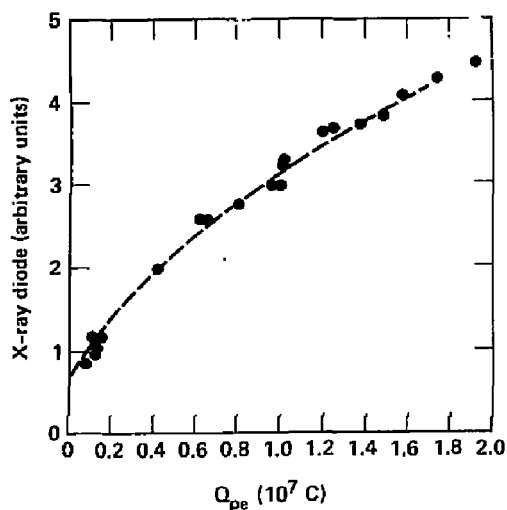
8

Fig. 6. Calibration curve of x-ray diode in terms of total photoelectron charge.

calibration curve is shown in Fig. 6, where we have plotted total photoelectron charge verses the x-ray diode response. The curvature at high fluxes is due to diode saturation.

The ratio of the total proton charge to photoelectron charge gives the probability of H^+ desorption per photoelectron. This desorption probability depends on the hydrogen surface coverage. Absolute cross sections can only be obtained by estimating the surface concentration of hydrogen. For these experiments we used the value of 2×10^{14} H/cm^2, which is consistent with a monolayer coverage.

Table 1 gives the values for the hydrogen desorption probabilities and absolute cross sections for the metal surfaces we studied. These are compared with values obtained by other workers studying low-energy-electron-stimulated desorption. These numbers are uncertain to the extent that surface coverage is uncertain. In fact, the increase in the desorption cross section from the low-Z to the high Z-coatings that we observe may be due to differences in the surface coverage. Therefore, we are currently attempting to measure the hydrogen surface coverage using thermal desorption techniques. These measurements will be described in a forthcoming paper.

9

Table 1. Hydrogen desorption probabilities and absolute cross sections.

Substrate	Ion	Probability (H^+/e^-)	Absolute cross section, σ_d $(cm^2)^a$	Electron energy	Reference
Be	H^+	4×10^{-10}	2×10^{-24}	>200 keV	This work
C	H^+	$8.38 \pm 1.38 \times 10^{-10}$	4×10^{-24}	>200 keV	This work
C	H^+	-	$\sim 10^{-22}$	<150 eV	Ref. 6
Al	H^+	2.5×10^{-10}	5×10^{-24}	>200 keV	This work
Ta	H^+	3×10^{-9}	6×10^{-23}	>200 keV	This work
W	H^+	-	3×10^{-21}	<150 eV	Ref. 7
Au	H^+	$1.93 \pm 0.17 \times 10^{-9}$	1×10^{-23}	>200 keV	This work

[a] Absolute cross sections based upon an assumed hydrogen surface coverage
of $2 \times 10^{14}/cm^2$.

4. DISCUSSION

X rays incident on, and passing through, a metal surface produce
electrons by photoelectric capture, Compton scattering, and pair production
(only possible at very high energy). These electrons, in turn, can desorb gas
molecules by exciting the surface bonds. The number of hydrogen atoms, Q_H,
removed by electron-stimulated desorption per incident flux of x rays is

$$Q_H = \Theta \int_0^\infty f(\varepsilon) \left[\int^{E_{max}} \eta(\varepsilon)\gamma(E)dE \right] d\varepsilon \quad , \qquad (5)$$

where Θ is the fraction of available desorption sites occupied by hydrogen
atoms, $f(\varepsilon)$ is the hydrogen yield per electron of energy ε for a fully
occupied surface, $\eta(\varepsilon)$ is the number of photoelectrons of energy ε
produced by an x ray of energy E, and $\gamma(E)$ is the number of photons with
energies between E and E + dE. Once $f(\varepsilon)$ and $\eta(\varepsilon)$ are known, Q_H can
be calculated for any x-ray spectrum and surface coverage.

10

The measurements of $f(\epsilon)$ and $n(\epsilon)$ are two separate problems. In this experiment, the double integral of $n(\epsilon)r(E)$ was measured directly and the energy distribution of the photoelectrons was later calculated using the SANDYL code.[3] The calculated photoelectron energy spectrum was used to give a spectrum-averaged desorption probability, P. Therefore, the total hydrogen yield can be calculated from

$$Q_H = \theta P N_\gamma Y \quad , \tag{6}$$

where N_γ is the x-ray fluence and Y is the total quantum yield (electrons/incident photon). This linearity between proton yield and photon flux is demonstrated in Fig. 7. Because the photoelectron energy spectrum is sharply peaked above 200 keV, the spectrum-averaged value, P, can be roughly equated to $f(\epsilon)\big|_{\epsilon = 200 \text{ keV}}$. This is not entirely correct, however, since we have not included the low-energy secondary electron flux that is present.

The desorption cross section $[\sigma_\theta \text{ (cm}^2)]$ is related to the desorption probability, $f(\epsilon)$, through the value of θ. If we assume that θ is equal to 1 in this experiment, then we obtain desorption cross sections of 10^{-23} to 10^{-24} cm^2. The electron impact ionization cross section for hydrogen
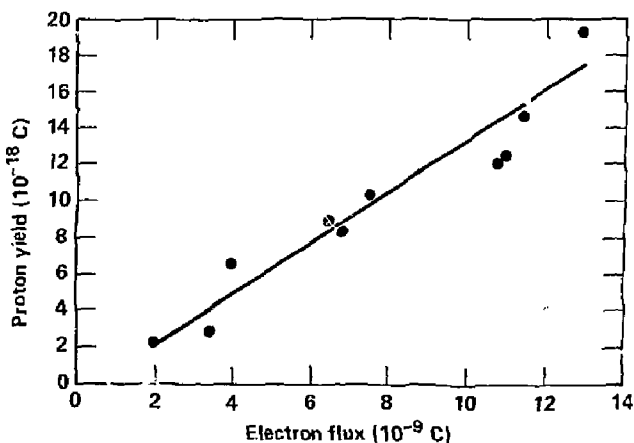
Fig. 7. Proton yield vs electron flux for desorption from a gold surface.

atoms in the gas phase is 1.0×10^{-19} cm^2 for 500-keV electrons.[8] Since the excitation mechanism may be similar for surface ionization and gas-phase ionization, the greatly reduced desorption cross sections must be the result of reneutralization of the hydrogen ions at the surface.

The ionic desorption cross section is related to the gas-phase ionization cross section, σ_0, by[9]

$$\sigma_d = \sigma_0 R \quad , \tag{7}$$

where R is the ion escape probability:

$$R = e^{-t_r/\tau} \quad , \tag{8}$$

where t_r is the time that the ion spends in the electronic interaction vicinity of the surface, and τ is the lifetime of the ionic state at the surface.

The lifetime of an excited atomic state at a free surface depends critically on both the distance of the adsorbed species from the surface and the electronic density of states of the metal. These, in turn, depend critically on surface structure as well as atomic number. Because of this, the desorption cross section is a function of surface preparation, and the results that are published here for deposited metal surfaces may not be correct for polycrystalline materials or single crystals.

We can estimate the lifetime of H$^+$ ions at a surface from the measured desorption cross sections using Eq. (8). First, we assume that the reneutralization matrix elements are position-independent over a distance of the order of 1Å. Second, we assume that the average escape energy of the hydrogen ions is 5 eV.[9-12] Then the residence time, t_R, is

$$t_R = \Delta X \, (2E_k/m_p)^{-1/2} = 3.2 \times 10^{-15} \text{ s} \quad , \tag{9}$$

where E_k is the escape energy ($\sim$5 eV), m_p is the rest mass of the hydrogen ion, and ΔX is the effective interaction distance ($\sim$1 Å). Using these values, we find that the lifetime of the excited hydrogen atom at the surface is of the order of 10^{-16} seconds. This is what is expected from quantum mechanical calculations, which predict lifetimes from 10^{-17} to 10^{-16} seconds.[13]

12

Before these results can be used to predict ion desorption yields for an arbitrary x-ray spectrum, it is necessary to know the energy dependence of the cross sections as well as the nature of the surface hydrogen coverage. We have already alluded to a method for extracting the energy dependence using Eq. (7) with the appropriate value for the reduction factor. If collective effects are unimportant, the reduction factor is, to first order, independent of the x-ray energy. Therefore, the energy dependence of the cross section should depend only on the gas-phase electron excitation cross section (assuming that the presence of a surface has little effect on the electronic wave functions of weakly bound adsorbates). In practice, however, Eq. (7) may be difficult to apply since it requires detailed information on the photoelectron energy spectrum as well as knowledge of the structure of the molecule giving rise to the desorption.

The photoelectron spectrum generated by the Febetron was determined up to 500 eV by reverse-biasing the extraction grid during the total charge measurements. The SANDYL calculations were used to extend the spectrum beyond 500 eV. A surprising result was that fewer than 5% of the photoelectrons had energies less than 200 eV; earlier experiments on photoelectron emission from gold indicated this percentage should be closer to 20%.[14]

Two possibilities come to mind which might explain the low secondary yield observed in these measurements. The first possibility is based upon the observation that during the total charge measurements the collector rapidly (in ~10 ns) reaches negative potentials larger than -20 V. Since the majority of the secondary electrons have energies less than this, they may be turned back before being collected. This does not affect the results of the cross-section measurements, however, because the desorption threshold is around 20 eV.[15] The second, and more interesting, possibility is that the presence of a thin coating reduces the escape of secondaries because of a change in the electronic density of states at the interface.

The appropriate gas-phase cross section to use in Eq. (7) depends upon what kind of electronic transition is responsible for desorption. Residual gas analysis of the vacuum used in our experiment indicated that the predominant source of hydrogen is water vapor. If the water vapor is simply physisorbed on the surface, then the electronic transition responsible for desorption of hydrogen would involve the fractionation of H_2O into a proton and an OH radical. Furthermore, a large H_2O^+ signal should be observed.

13

On the other hand, if H_2O dissociates on the surface, then protons might originate from impact ionization and fragmentation of OH on the surface. The observation that the threshold energy for desorption is greater than 30 eV makes it unlikely that desorption is due to impact ionization of atomic hydrogen. Instead, this high threshold energy indicates that a two-electron transition may be occurring. Furthermore, the 5-6-eV proton energies are much greater than the predictions of Thomas-Fermi models for bare protons desorbing from a surface.[16]

A more likely case can be made for the fragmentation of OH radicals. First is the observation from the data that the predominant desorbed ion species are H^+, H_2^+, and OH^+. Very few H_2O^+ ions are observed. Second, physisorbed H_2O molecules are not usually stable on clean surfaces above room temperature. If an oxide surface is present, as it definitely is with the beryllium, aluminum, and tantalum surfaces, the H_2O molecule dissociates into a chemisorbed OH radical.[17-19] The reaction is

$$H_2O_{(g)} + O_{(a)} \longrightarrow 2\ OH_{(a)} \quad . \tag{10}$$

The small presence of H_2O that is observed in the time-of-flight spectra may be due to ionization of any H_2O formed by the back-reaction to Eq. (10). H_2 most likely is formed by ionization and fragmentation of hydrocarbons.

5. CONCLUSION

We have measured the desorption cross sections for hydrogen ions from beryllium, carbon, aluminum, tantalum, and gold surfaces. The results of the studies give values for the cross sections ranging between 2×10^{-24} cm^2 and 6×10^{-23} cm^2. The increase in the desorption cross section with increasing Z of the substrate may not be a property of the desorption kinetics; rather, it may be due to differences in the hydrogen surface coverage that we have not accounted for. This will be the subject of another study.

The small cross sections, as well as the lack of H_2O^+ ions in the desorption mass spectra, indicate that the hydrogen ions originate from the fragmentation of chemisorbed OH radicals. These OH radicals are formed at room temperature when H_2O molecules impinge upon a surface that has an oxide covering.

14

6. REFERENCES

1. S. Brumbach and M. Kaminsky, <u>J. Nucl. Mat.</u> <u>63</u>, 188 (1976).

2. B. L. Pruett, private communication, Lawrence Livermore National Laboratory.

3. C. Cerjan, private communication, Lawrence Livermore National Laboratory.

4. J. H. Kinney, unpublished.

5. J. L. Wiza, <u>Nucl. Inst. Meth.</u> <u>162</u>, 587 (1979).

6. M. I. Datsiev and Y. I. Belyakov, <u>Sov. Phys. Tech. Phys.</u> <u>14</u>, 848 (1969).

7. M. Nishijima and F. M. Propst, <u>Phys. Rev.</u> <u>B2</u>, 2368 (1970).

8. C. F. Barnett, J. A. Ray, E. Ricci, M. I. Wilker, E. W. McDaniel, E. W. Thomas and H. B. Gilbody, in <u>Atomic Data for Controlled Fusion Research</u>, Oak Ridge National Laboratory, Oak Ridge, TN, ORNL-5207 Vol. 2 (1977).

9. T. E. Madey and J. T. Yates, Jr., <u>J. Vac. Sci. Tech.</u> <u>8</u>, 525 (1971).

10. J. H. Leck and B. P. Stimpson, <u>J. Vac. Sci. Tech.</u> <u>9</u>, 293 (1971).

11. P. A. Redhead, <u>Nuovo Cimento Suppl.</u> <u>5</u>, 586 (1967).

12. E. Bauer and H. Poppa, <u>Surf. Sci.</u> <u>99</u>, 341 (1980).

13. M. Tsukada and W. Brenig, <u>Z. Phys. B</u> <u>23</u>, 369 (1976).

14. J. L. Gaines and R. A. Hansen, <u>J. Applied Phys.</u> <u>47</u>, 3923 (1976).

15. M. J. Drinkwine, "Bombarding Electron Energy Effects in Electron Stimulated Desorption Studies. Electron energies: 50-6000 eV," Ph.D. thesis, University of Wisconsin, Milwaukee, WI (1977).

16. J. H. Kinney, unpublished.

17. A. Spitzer, A. Ritz, and H. Lüth, <u>Surf. Sci.</u> <u>152/153</u>, 543 (1985).

18. E. M. Stuve, S. W. Jorgensen, and R. J. Madix, <u>Surf. Sci.</u> <u>146</u>, 179 (1984).

19. K. Bange, T. E. Madey, and J. K. Sass, <u>Surf. Sci.</u> <u>152/153</u>, 550 (1985).

CONTENTS

DISCLAIMER